MOSARIX: Multi-crystal spectrometer in the tender x-ray range at SOLEIL synchrotron

Iyas Ismail, Roba Moussaoui, Régis Vacheresse, Tatiana Marchenko, Oksana Travnikova, Renaud Guillemin, Abhishek Verma, Nicolas Velasquez, Dawei Peng, Hugues Ringuenet, et al.

MOSARIX: Multi-Crystal Spectrometer in the Tender X-ray Range at SOLEIL Synchrotron

Iyas Ismail,[1] Roba Moussaoui,[1] Régis Vacheresse,[1] Tatiana Marchenko,[1] Oksana Travnikova,[1] Renaud Guillemin,[1] Abhishek Verma,[1] Nicolas Velasquez,[1] Dawei Peng,[1] Hugues Ringuenet,[1] Francis Penent,[1] Ralph Püttner,[2] Denis Céolin,[3] Jean-Pascal Rueff,[1,3] and Marc Simon[1]

[1)] *Sorbonne Université, CNRS, UMR 7614, Laboratoire de Chimie Physique-Matière et Rayonnement, 4 Place Jussieu, 75252 Paris, France.*

[2)] *3Fachbereich Physik, Freie Universität Berlin, Arnimallee 14, D-14195 Berlin, Germany.*

[3)] *Synchrotron SOLEIL, l'Orme des Merisiers, Saint-Aubin, BP 48, F-91192 Gif-sur-Yvette Cedex.*

(*Electronic mail: iyas.ismail@sorbonne-universite.fr)

(Dated: 26 April 2024)

We have built and commissioned a novel standalone multi-crystal x-ray spectrometer (MOSARIX) in the von Hamos configuration based on highly annealed pyrolytic graphite (HAPG) crystals. The spectrometer is optimized for the energy range of 2 to 5 keV, but this range can be extended up to 20 keV by using higher reflection orders. With its nine crystals and a Pilatus detector, MOSARIX achieves exceptional detection efficiency with good resolving power (better than 4000), opening the door to study small cross-section phenomena and to perform fast in-situ measurements. The spectrometer operates under a He atmosphere, which provides a flexible sample environment for measurements in gas, liquid, and solid phases.

I. INTRODUCTION

Recent advancements in X-ray source technology, including third and fourth-generation synchrotrons and X-ray free electron lasers (XFEL), have significantly expanded the possibilities for exploring novel phenomena. For instance, studies on double-core-hole states, ultrafast nuclear dynamics, ultrafast charge transfer and postcollision-interaction effects[1–3]. This progress has furthered the development of resonant inelastic X-ray scattering (RIXS), a powerful technique for investigating atoms, molecules, liquids, and solids. RIXS has been largely used with soft[4] and hard[5] X-rays which enables studies on interactions with core-level electrons and providing chemical sensitivity across a wide range of applied studies, including solar cells and fundamental research[6]. In the region between soft and hard X-rays, namely, the tender X-ray regime (2-5 keV), the RIXS technique has been less explored, one of the reasons being the lack of efficient position-sensitive detectors in this energy range. This prompted the development of our first spectrometer, operating in the von Hamos geometry within the 2-5 keV energy range at the SOLEIL synchrotron facility[7]. This energy range enables investigations at the K-edge of elements, from phosphor to vanadium, and at the L-edge of elements, spanning from zirconium to platinum. The spectrometer was equipped with one HAPG crystal combined to a microchannel plate-based detector including a photocathode[8]. Its operation took place under high-vacuum conditions more details can be found in Ref.[7]. The success of this spectrometer has encouraged us to push the boundaries further, aiming to develop a spectrometer that offers significantly enhanced efficiency and flexibility, capable of accommodating samples in various states (liquid, solid, and gas). These extended capabilities enable also an easy in-operando measurements which is of great importance in various fields, particularly for battery development[9].

We present here this new instrument in details together with the first results obtained, namely the K_β RIXS 2D map of native sulfur solid sample measured at the sulfur K edge, as well as K_α RIXS 2D map of $FeCl_3$ in a water solution obtained with a microliquid jet.

II. TECHNICAL DESCRIPTION

The design of the present instrument is directly inspired by our first one-crystal spectrometer. For a more comprehensive description of the crystal selection and geometry impact on the spectrometer performances, please refer to Ref[7]. Here, we recall some necessary information and present essential new design points, particularly the multi-crystal and the under-helium operation features.

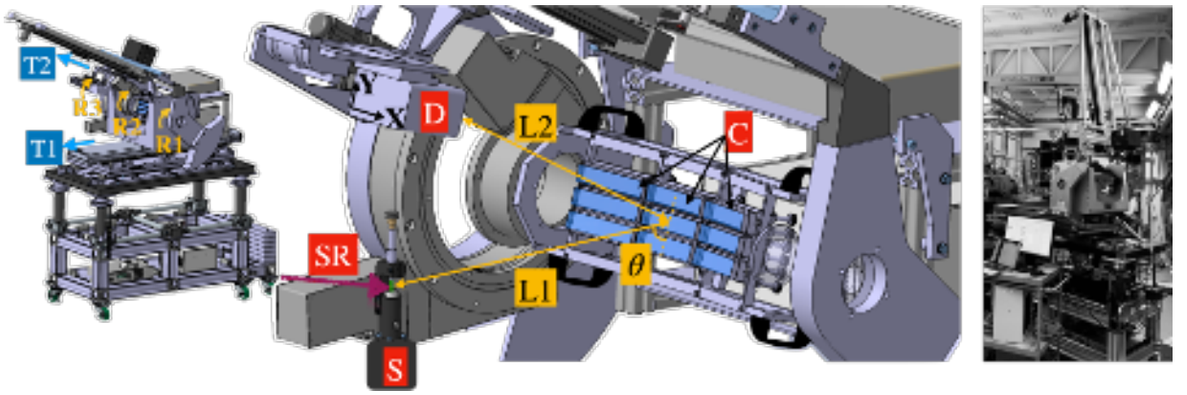

FIG. 1. (left) A 3D view of the spectrometer highlighting its main mechanical components, mainly the three rotation stages R1, R2 and R3 (yellow curved arrows) and the two translation stages T1 and T2 (blue arrows). (middle) A close-up view showing the nine crystals (C), the detector (D), and the micro-liquid jet sample (S), all positioned at the distances required for achieving the focalizing condition L1=L2=R/sin (θ). θ is the Bragg angle. (SR) is the incoming photon beam. (right) a photo of the spectrometer.

A. Multi-crystal

In the von Hamos geometry, a cylindrically curved crystal is employed, which defines two distinct planes [10,11]. In the focusing plane, the diffracted X-rays are optimally focalized onto a point along the detector x axis. This occurs when both the detector and the X-ray source (sample) are precisely positioned at the crystal curvature radius (R), i.e., L1=L2=R/sin (θ) where θ is the (central) Bragg angle, L1 is distance from crystal to sample and L2 is distance from crystal to detector (Fig. 1). In contrast, within the dispersive plane, the crystal behaves as a flat crystal. Consequently, photons of varying energies are diffracted at distinct angles, resulting in different positions along the detector y axis, in accordance with the Bragg law.

To enhance the spectrometer efficiency, one can increase either the solid angle or the crystal reflectivity. Several methods have been developed to expand the solid angle, such as using up to 16 crystals[12], employing a large segmented-crystal[13], or even implementing a full-cylindrical crystal[14]. All of these spectrometers are optimized for X-ray emission spectroscopy in the 5-10 keV range. On the other hand, mosaic crystals are known of achieving higher reflectivity. This is demonstrated by the recent implementation of graphite mosaic crystals in a von Hamos geometry spectrometer for measuring X-rays in the range of 4.5-10 keV[15,16] and 8-60 keV[17].

In this work, we combined two approaches to enhance the spectrometer efficiency by increasing both the solid angle and the crystal reflectivity. We employed nine Highly Annealed Pyrolytic Graphite (HAPG) crystals, each with dimensions of a = 25 mm along the dispersive direction, b= 110 mm in the non-dispersive direction, and a radius of curvature R = 500 mm. Each crystal is made of a N-BK7 glass substrate coated with a 40 μm thick layer of HAPG material by the Optigraph company. This design provides a large solid angle of up to $\Omega \sim 90$ msr, resulting in a solid angle per eV of $\Omega/\text{eV} \sim 2.5$ msr/eV. Figure 2.d shows calculated values of both the solid angle and the solid angle per eV for different (central) energies and different orders of reflections. A Pilatus 100K-M detector equipped with a low-energy detection capability, enables the measurement of the position (x, y) of the photons starting from 2 keV energy. The detector active surface consists of 487 pixels × 195 pixels, with each pixel measuring 172 × 172 μm^2. Considering the pixel size of the detector together with the source size(20 μm), the crystal mosaicity[7] and the intrinsic broadening of the Bragg reflection ($\Delta\theta/\theta = 2.6 \times 10^{-4}$)[18], we calculated the energy resolution of the spectrometer (Fig. 2.c). Figure 3 shows measured elastic peaks from a water liquid sample, produced using the micro-liquid jet system detailed later. The photon energy was varied with a step width of 5 eV from 3920 to 3945 eV. The spectrometer operated using the 2nd order of reflection at a Bragg angle of 71.41°. The resulting spectrum was fited with the sum of Gaussian functions, yielding a full width at half maximum (FWHM) of 1.12 eV. With a photon bandwidth of the beamline (0.7 eV), we derived a spectrometer resolution of 0.87 eV, corresponding to a resolving power of E/ΔE = 4500.

The main advantage of the von Hamos geometry is its capability to capture single-shot spectra without the need for any scanning components. The spectrometer can be configured to measure a certain energy window, which is limited mainly by the crystal width. Figure 2.b shows calculated values of spectrometer energy window width for different (central) photon energies and different reflection orders.

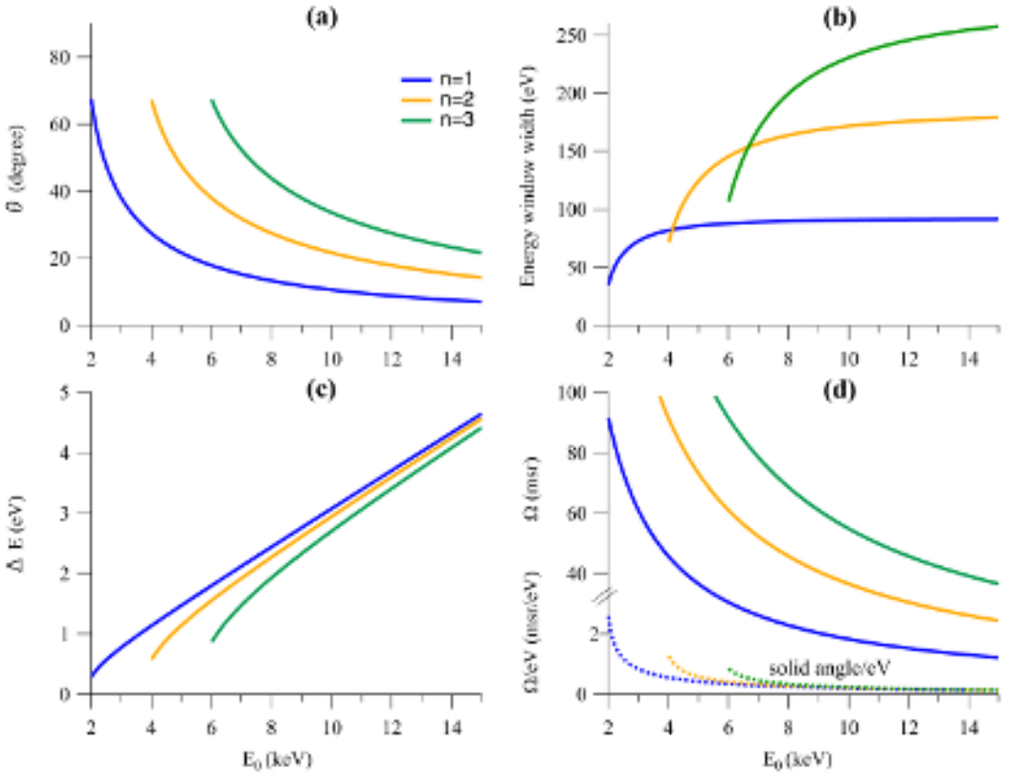

FIG. 2. Calculated (a) Bragg angle (b) spectrometer energy window width (c) energy resolution (d) solid angle (Ω) and solid angle per eV (dashed lines) for different (central) photon energies (E_0) and different reflection orders (n).

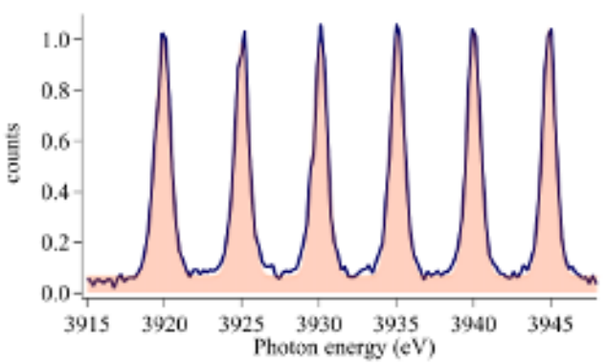

FIG. 3. Elastic peaks from a water liquid sample measured by changing the photon energy with a step width of 5 eV from 3920 to 3945 eV using the 2nd order of reflection at Bragg angle 71.41°. The shaded area indicates the result of the fitting procedure with the sum of Gaussian functions.

B. Mechanical design

The nine crystals are arranged in a 3×3 array, which diffracts and focuses the photons from the sample onto a 2D detector following Bragg law, $n\lambda = 2d \sin\theta$. Each crystal is equipped with three motors, allowing for individual fine alignment, especially fine adjustments of the pitch (Bragg angle) and yaw angles. The displacement of the three motors in the same direction allows the alignment of the spectrum of each crystal along the dispersion axis. The alignment of the spectrometer is fully computer-controlled. As shown in Fig. 1, the crystal array is placed on a rotating stage (R2) for selecting the central Bragg angle (θ). The detector is positioned on both translation (T2) and rotation (R1) stages for precise adjustment of the (2θ) angle and crystal-detector (L2) distance. Achieving focalization is possible with a second translation stage (T1), accommodating the entire spectrometer. These two translation stages allow

fine-tuning of the source-crystal (L1) and crystal-detector (L2) distances. In addition, the detector can be oriented parallel to the crystal surface using a rotation stage (R3).

We have developed a dedicated python-based software to calculate the spectrometer motor parameters, featuring a user-friendly interface that simplifies the process to selecting the desired energy range. However, some fine adjustment of the crystals may still be necessary. This software efficiently controls all the 32 motors and is designed for accessibility to non-expert users. It is important to note that crystals can be aligned in two different ways. First, the signals of the individual crystals can be imaged as individual spectra as shown in Fig. 4. Second, the signals of the crystals can be aligned so that they produce one overlapping spectrum. With the latter, the signal-to-noise ratio is enhanced but potentially compromising spectral resolution due to possible misalignments.

It is important to note that the resolution of mosaic crystals significantly depends on the quality of alignment, particularly satisfying the focusing conditions. Moreover, since the crystals are not perfectly identical, slight differences in resolution between them may be observed. In this regard, when recording separate spectra, we have the option, in the post-measurement-treatment, to consider only the contribution of the best crystals if the resolution is our primary focus. We found that when the crystals are well-aligned so that their corresponding spectral resolutions are the same, the summation procedure of the individual spectra does not affect the overall spectral resolution.

C. He balloon

The spectrometer operates within a helium atmosphere, a decision due to the extremely low transmission of 1 m of air at ambient pressure 2 keV and 4 keV, which is about 4.10^{-28} and 4.10^{-9}, respectively[19]. In contrast to this, the attenuation within He atmosphere is almost negligible. To prevent any loss of intensity, or artifacts possibly caused by window materials and impurities, the entire spectrometer components (crystals and detector) and the sample are enclosed within a helium balloon. This arrangement ensures that photons emitted from the sample encounter only helium without any additional windows. For this purpose, a large, flexible balloon, made of thermoplastic polyurethane (TPU), was specially designed with dedicated feedthroughs, allowing the passage of various cables and tubes, which are necessary to operate the sample holder, the liquid jet or the gas cell, from the exterior to the interior of the balloon. A glovebox-style manipulator was also implemented to facilitate sample changes and manipulations without disrupting the helium atmosphere. Additionally, a helium detector was integrated to provide real-time measurements and monitoring of helium concentration. This flexible design, in every sense, enables seamless work with solid, liquid, and gas-phase samples, allowing even rapid exchange between them.

D. Data treatment: pymosarix package

We have developed a dedicated Python package for processing spectrometer data. The package is named pymosarix and can be installed from Ref.[20]. As mentioned earlier, data are recorded using the separate spectra configuration. In this case, the initial step of the treatment involves selecting the regions-of-interest (ROIs) corresponding to each spectrum (from each crystal) on the image provided by the detector. In the second step, the calibration curve (pixel scale to energy scale) for each spectrum needs to be determined. This is usually performed by measuring the elastic peak at selected photon energies covering the energy range of interest. An automated procedure allows for the collection, processing, and determination of the calibration parameters for each crystal from the elastic peak measurements. Based on this calibration, the software converts the spectra from pixel scale to energy scale. With the spectra now aligned in the energy scale, they can be directly summed. The package also includes additional features for rapid fitting and the construction of RIXS 2D maps.

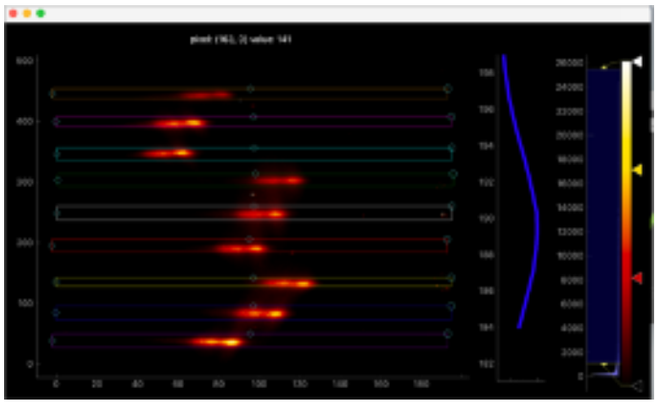

FIG. 4. A pymosarix software screenshot showing a typical detector image with nine spots, each corresponding to emission spectra diffracted by individual crystals.

III. RESULTS AND DISCUSSIONS

The spectrometer was commissioned in the RIXS hutch of the GALAXIES beamline at SOLEIL synchrotron. The beamline operates in the 2.3 to 12 keV energy range with high flux and high resolution. The beamline description has been published elsewhere[21]. The MOSARIX spectrometer used the same sample stage as the beamline RIXS spectrometer. Due to constraints related to the existing RIXS spectrometer the MOSARIX spectrometer was positioned at an angle of 124°, in the horizontal plane, relative to the incident direction of the horizontally linear-polarized synchrotron light. This limits the ability to operate the spectrometer at different angles (notably 0°, 55°, and 90°), which could be advantageous, for instance, in minimizing the contribution of the elastic peak (at 90°). The x-ray beam was focused to ∼20 (V)×80 (H) μm^2 to deliver a total flux of ∼ 10^{13} photons/s at a ring current of 450 mA. The monochromator energy was calibrated to the first derivative of the Fe edge from a metallic Fe foil (7112 eV). For each energy set, the elastic scattering peak was recorded for several incident photon energies to calibrate the spectrometer. The pymosarix package was used for the calibration and data treatment.

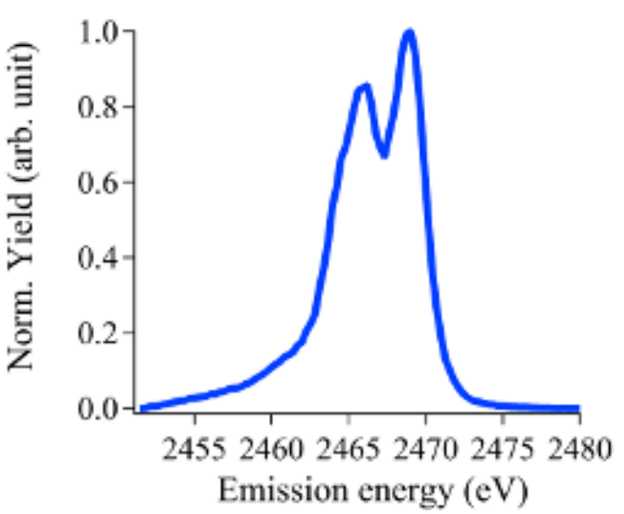

FIG. 5. Sulfur K$_\beta$ emission spectrum measured at incident photon energy of 4300 eV

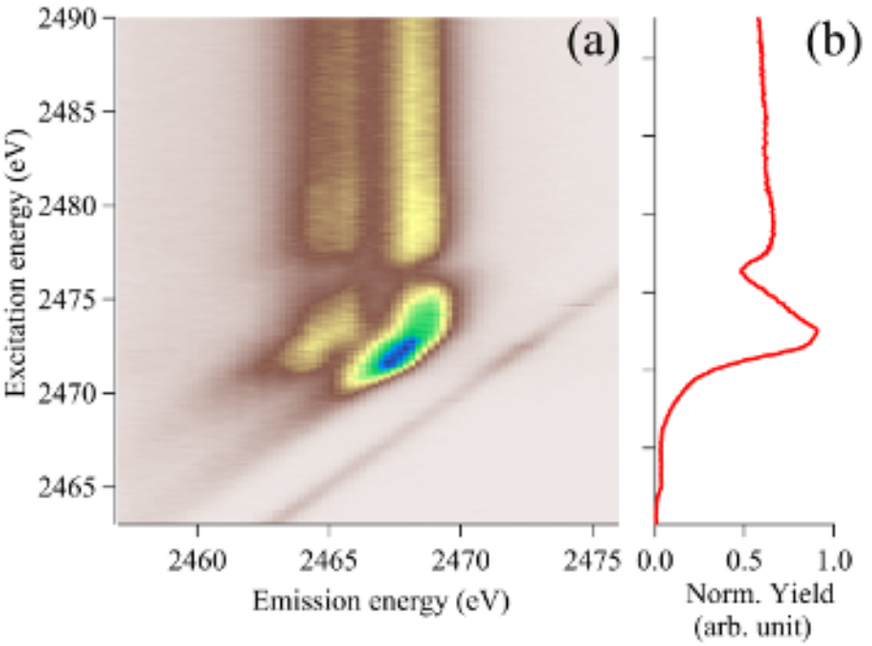

FIG. 6. (a) RIXS 2D map of native sulfur K_β emission at the K edge. (b) absorption spectrum obtained by integrating the RIXS 2D map over 2462- 2469 eV emitted photon energies.

A. Solid sulfur

Native sulfur purchased from Sigma Aldrich (purity 99.998%) was placed on a computer-controlled sample holder and exposed to sychrotron radiation. The spectrometer was set to measure the sulfur K_β emission ($\sim$ 2465 eV) at a Bragg angle of 48.71°. The incoming photon energy was tuned to 4300 eV, i.e., above the sulfur K edge. Figure 4 shows a screen shoot taken from pymosarix software showing a typical image from the detector. We can observe the nine spots corresponding to emission spectra diffracted by the nine crystals. For each crystal, selected ROI is delimitated by a colored rectangle. Each individual spectrum is obtained by integrating the corresponding sub-image defined by the selected ROI, along the vertical axis. The spectra are then calibrated in energy and the resulted spectrum, shown in Fig. 5, is in agreement with Ref.[22].

Figure 6.a shows a 2D RIXS 2D map of sulfur K_β emission excited at the S K-edge. The map was recorded by changing the photon beam energy from 2460 eV to 2490 eV with a step width of 0.1 eV. The total acquisition time was about 60 minutes. The straight diagonal line with the slope of one corresponds to the elastic peak and demonstrates the quality of the energy calibration. The absorption spectrum, obtained by integrating the RIXS over the emitted photon energies range of 2462-2465eV, (Fig. 6.b) is in perfect agreement with the Ref.[23].

B. Aqueous solution of $FeCl_3$

The measurement was conducted using a simplified version of the microliquid jet system developed at the GALAXIES beamline[24]. A 1.0 M $FeCl_3$ aqueous solution was injected into the capillary using a high-performance liquid chromatography (HPLC) pump, maintaining a constant flux of 1.6 ml/min. The $FeCl_3$ solution was prepared by mixing $FeCl_3$ salt (purity 99%) with deionized water. Prior to injection, filtering and degassing procedures were systematically performed.

The spectrometer was configured to measure Fe K_α emissions using the 3rd order of reflection of the spectrometer at Bragg angle 60.04°. Figure 7 shows the corresponding 2D RIXS 2D map using the excitation energy range between 7110 eV and 7200 eV, i.e. mainly around 1s $\longrightarrow$ 4p excitation energy, and a step width of 0.5 eV. The data acquisition for the map took 90 minutes. The emitted energies are in good agreement with Ref.[25] measured at 1s $\longrightarrow$ 3d excitation energy.

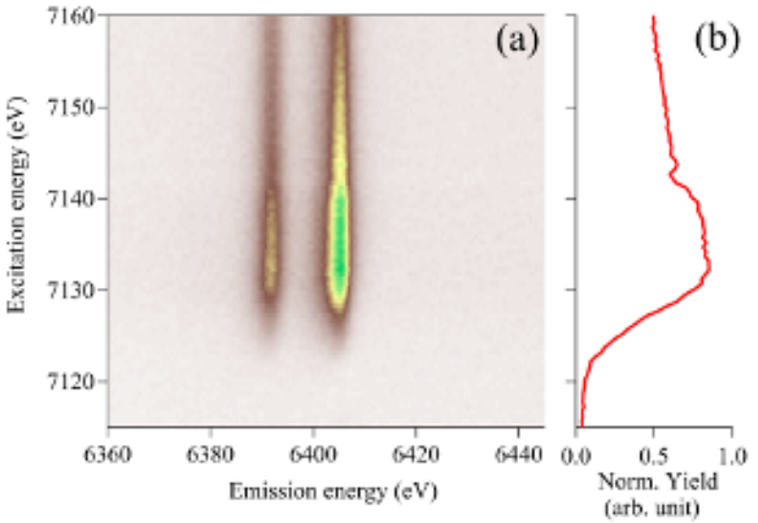

FIG. 7. (a) RIXS 2D map of the 1M-solution of $FeCl_3$ K_α emission at the Fe K edge. (b) absorption spectrum obtained by integrating the RIXS 2D map over emitted photon energies.

IV. CONCLUSION

We have developed a standalone portable multi-crystal wavelength-dispersive spectrometer for the tender x-ray range. This fully computer-controlled spectrometer is equipped with a 2D position-sensitive detector enabling high repetition rates necessary for operation at synchrotron radiation facilities and free-electron-laser sources. MOSARIX stands out with its remarkable efficiency, thanks to a wide collection angle of up to ~ 90 msr (2.5 msr/eV) and the high integrated reflectivity of the HAPG crystals, combined with good energy resolution. These features enable studies of very low cross-section phenomena, such as e.g. double-core-hole states [26], and allows extending implementation of RIXS technique to the tender x-rays range, as well as to liquid and gas samples. This flexibility is made possible by the very versatile design of the spectrometer. The crystals can be arranged in different configurations to record separate individual spectra or a combined spectrum. It should be mentioned that aligning the spectrometer is time-consuming, often taking up to several hours. When working with the individual spectra configuration, the focus is primarily on optimizing the resolution of each crystal, although some differences can be tolerated. Changing the central photon energy can be accomplished without major realignment in certain cases. In contrast, working with the combined spectrum configuration is more complex and time-consuming because it requires additional task to perfectly superpose the spectra from each crystal on the detector. In addition, crystals of different types can be installed to monitor different energy windows simultaneously. Finally, The spectrometer can be used to study gas-phase samples using a similar gas cell as the one we developed for the RIXS spectrometer[27].

Currently, this instrument is in operation at the GALAXIES beamline of SOLEIL synchrotron radiation facility and is open to external users through the standard SOLEIL call for proposals procedure.

ACKNOWLEDGMENTS

Experiments were performed on the GALAXIES beam line at SOLEIL Synchrotron, France (Proposals No. 99230105 and No. 20220383). We are grateful to Dominique PRIEUR for technical support and to SOLEIL staff for smoothly running the facility. N.V. and T.M. acknowledge funding from the European Union's Horizon 2020 research and innovation program under the Marie Sklodowska-Curie grant agreement No [860553]. We are grateful to David MASSOT for his invaluable administrative support. This work was performed within the LABEX Plas@Par project supported by Grant No. 11-IDEX0004-02 from Agence Nationale de la Recherche.

DATA AVAILABILITY STATEMENT

The data are available from the authors upon reasonable request.

[1]M. N. Piancastelli, T. Marchenko, R. Guillemin, L. Journel, O. Travnikova, I. Ismail, and M. Simon, "Hard x-ray spectroscopy and dynamics of isolated atoms and molecules: a review," Reports on Progress in Physics **83**, 016401 (2019).
[2]N. Velasquez, O. Travnikova, R. Guillemin, I. Ismail, L. Journel, J. B. Martins, D. Koulentianos, D. Céolin, L. Fillaud, M. L. M. Rocco, R. Püttner, M. N. Piancastelli, M. Simon, S. Sheinerman, L. Gerchikov, and T. Marchenko, "Generalization of the post-collision interaction effect from gas-phase to solid-state systems demonstrated in thiophene and its polymers," Phys. Rev. Res. **5**, 013048 (2023).
[3]I. Ismail, A. Ferté, F. Penent, R. Guillemin, D. Peng, T. Marchenko, O. Travnikova, L. Inhester, R. Taïeb, A. Verma, N. Velasquez, E. Kukk, F. Trinter, D. Koulentianos, T. Mazza, T. M. Baumann, D. E. Rivas, Y. Ovcharenko, R. Boll, S. Dold, A. De Fanis, M. Ilchen, M. Meyer, G. Goldsztejn, K. Li, G. Doumy, L. Young, G. Sansone, R. Dörner, M. N. Piancastelli, S. Carniato, J. D. Bozek, R. Püttner, and M. Simon, "Alternative pathway to double-core-hole states," Phys. Rev. Lett. **131**, 253201 (2023).
[4]J. Nordgren, G. Bray, S. Cramm, R. Nyholm, J.-E. Rubensson, and N. Wassdahl, "Soft x-ray emission spectroscopy using monochromatized synchrotron radiation," Review of Scientific Instruments **60**, 1690–1696 (1989).
[5]J.-P. Rueff and A. Shukla, "Inelastic x-ray scattering by electronic excitations under high pressure," Reviews of Modern Physics **82**, 847 (2010).
[6]T. Marchenko, L. Journel, T. Marin, R. Guillemin, S. Carniato, M. Žitnik, M. Kavčič, K. Bučar, A. Mihelič, J. Hoszowska, W. Cao, and M. Simon, "Resonant inelastic x-ray scattering at the limit of subfemtosecond natural lifetime," The Journal of Chemical Physics **134**, 144308 (2011), https://pubs.aip.org/aip/jcp/article-pdf/doi/10.1063/1.3575514/14066501/144308_1_online.pdf.
[7]I. Ismail, L. Journel, R. Vacheresse, O. Travnikova, T. Marin, D. Céolin, R. Guillemin, T. Marchenko, M. Zmerli, D. Koulentianos, R. Püttner, J. Palaudoux, F. Penent, and M. Simon, "A von Hamos spectrometer based on highly annealed pyrolytic graphite crystal in tender x-ray domain," Review of Scientific Instruments **92**, 073104 (2021), https://pubs.aip.org/aip/rsi/article-pdf/doi/10.1063/5.0054421/16016765/073104_1_online.pdf.
[8]I. Ismail, L. Journel, R. Vacheresse, J. Palaudoux, T. Marin, F. Penent, and M. Simon, "Time and position sensitive photon detector for coincidence measurements in the kev energy range," Review of Scientific Instruments **89** (2018).
[9]S. Saha, G. Assat, M. T. Sougrati, D. Foix, H. Li, J. Vergnet, S. Turi, Y. Ha, W. Yang, J. Cabana, et al., "Exploring the bottlenecks of anionic redox in li-rich layered sulfides," Nature Energy **4**, 977–987 (2019).
[10]L. v. Hámos, "Röntgenspektroskopie und abbildung mittels gekrümmter kristallreflektoren," Naturwissenschaften **20**, 705–706 (1932).
[11]J. Hoszowska, J. C. Dousse, J. Kern, and C. Rhême, "High-resolution von hamos crystal x-ray spectrometer," Nuclear Instruments and Methods in Physics Research Section A: Accelerators, Spectrometers, Detectors and Associated Equipment **376**, 129–138 (1996).
[12]R. Alonso-Mori, J. Kern, D. Sokaras, T.-C. Weng, D. Nordlund, R. Tran, P. Montanez, J. Delor, V. K. Yachandra, J. Yano, et al., "A multi-crystal wavelength dispersive x-ray spectrometer," Review of Scientific Instruments **83** (2012).
[13]J. Szlachetko, M. Nachtegaal, E. de Boni, M. Willimann, O. Safonova, J. Sa, G. Smolentsev, M. Szlachetko, J. A. van Bokhoven, J.-C. Dousse, J. Hoszowska, Y. Kayser, P. Jagodzinski, A. Bergamaschi, B. Schmitt, C. David, and A. Lücke, "A von Hamos x-ray spectrometer based on a segmented-type diffraction crystal for single-shot x-ray emission spectroscopy and time-resolved resonant inelastic x-ray scattering studies," Review of Scientific Instruments **83**, 103105 (2012), https://pubs.aip.org/aip/rsi/article-pdf/doi/10.1063/1.4756691/14133709/103105_1_online.pdf.
[14]W. Malzer, D. Grötzsch, R. Gnewkow, C. Schlesiger, F. Kowalewski, B. Van Kuiken, S. DeBeer, and B. Kanngießer, "A laboratory spectrometer for high throughput x-ray emission spectroscopy in catalysis research," Review of Scientific Instruments **89** (2018).
[15]L. Jarrott, M. Wei, C. McGuffey, F. Beg, P. Nilson, C. Sorce, C. Stoeckl, W. Theoboald, H. Sawada, R. Stephens, et al., "Calibration and characterization of a highly efficient spectrometer in von hamos geometry for 7-10 kev x-rays," Review of Scientific Instruments **88** (2017).
[16]U. Zastrau, A. Woldegeorgis, E. Förster, R. Loetzsch, H. Marschner, and I. Uschmann, "Characterization of strongly-bent hapg crystals for von-hámos x-ray spectrographs," Journal of Instrumentation **8**, P10006 (2013).
[17]M. Gerlach, L. Anklamm, A. Antonov, I. Grigorieva, I. Holfelder, B. Kanngießer, H. Legall, W. Malzer, C. Schlesiger, and B. Beckhoff, "Characterization of hapg mosaic crystals using synchrotron radiation," Journal of Applied Crystallography **48**, 1381–1390 (2015).
[18]G. Ice and C. Sparks, "Mosaic crystal x-ray spectrometer to resolve inelastic background from anomalous scattering experiments," Nuclear Instruments and Methods in Physics Research Section A: Accelerators, Spectrometers, Detectors and Associated Equipment **291**, 110–116 (1990).
[19]B. L. Henke, E. M. Gullikson, and J. C. Davis, "X-ray interactions: photoabsorption, scattering, transmission, and reflection at e= 50-30,000 ev, z= 1-92," Atomic data and nuclear data tables **54**, 181–342 (1993).
[20]"Python package pymosarix," .
[21]J.-P. Rueff, J. Ablett, D. Céolin, D. Prieur, T. Moreno, V. Balédent, B. Lassalle-Kaiser, J. Rault, M. Simon, and A. . Shukla, "The galaxies beamline at the soleil synchrotron: inelastic x-ray scattering and photoelectron spectroscopy in the hard x-ray range," Journal of synchrotron radiation **22**, 175–179 (2015).
[22]M. Kavcic, M. Petric, A. Rajh, K. Isakovic, A. Vizintin, S. D. Talian, and R. Dominko, "Characterization of li–s batteries using laboratory sulfur x-ray emission spectroscopy," ACS applied energy materials **4**, 2357–2364 (2021).
[23]M. Kavcic, K. Bucar, M. Petric, M. Zitnik, I. Arcon, R. Dominko, and A. Vizintin, "Operando resonant inelastic x-ray scattering: An appropriate tool to characterize sulfur in li–s batteries," The Journal of Physical Chemistry C **120**, 24568–24576 (2016).
[24]T. Miteva, N. V. Kryzhevoi, N. Sisourat, C. Nicolas, W. Pokapanich, T. Saisopa, P. Songsiriritthigul, Y. Rattanachai, A. Dreuw, J. Wenzel, et al., "The all-seeing eye of resonant auger electron spectroscopy: a study on aqueous solution using tender x-rays," The Journal of Physical Chemistry Letters **9**, 4457–4462 (2018).
[25]M. Bauer and C. Gastl, "X-ray absorption in homogeneous catalysis research: the iron-catalyzed michael addition reaction by xas, rixs and multi-dimensional spectroscopy," Physical Chemistry Chemical Physics **12**, 5575–5584 (2010).
[26]J. Hoszowska, J. C. Dousse, W. Cao, K. Fennane, Y. Kayser, M. Szlachetko, J. Szlachetko, and M. Kavčič, "Double k-shell photoionization and hypersatellite x-ray transitions of $12 \leq z \leq 23$ atoms," Physical Review A **82**, 063408 (2010).
[27]I. Ismail, R. Guillemin, T. Marchenko, O. Travnikova, J. Ablett, J.-P. Rueff, M.-N. Piancastelli, M. Simon, and L. Journel, "Experimental setup for the study of resonant inelastic x-ray scattering of organometallic complexes in gas phase," Review of Scientific Instruments **89** (2018).